Bioorganic & Medicinal Chemistry 28 (2020) 115598

Contents lists available at ScienceDirect

Bioorganic & Medicinal Chemistry

journal homepage: www.elsevier.com/locate/bmc

Structural studies of triazole inhibitors with promising inhibitor effects against antibiotic resistance metallo-β-lactamases

Zeeshan Muhammad[a], Susann Skagseth[b], Marc Boomgaren[a], Sundus Akhter[a], Christopher Fröhlich[b], Aya Ismael[a], Tony Christopeit[b], Annette Bayer[a,*], Hanna-Kirsti S. Leiros[b,*]

[a] Department of Chemistry, Faculty of Science and Technology, UiT The Arctic University of Norway, N-9037 Tromsø, Norway
[b] The Norwegian Structural Biology Centre (NorStruct), Department of Chemistry, Faculty of Science and Technology, UiT The Arctic University of Norway, N-9037 Tromsø, Norway

ARTICLE INFO

Keywords:
Metallo-β-lactamase inhibitor
*N*H-triazole
Inhibition properties
Crystal structure
Structural guided design

ABSTRACT

Metallo-β-lactamases (MBLs) are an emerging cause of bacterial antibiotic resistance by hydrolysing all classes of β-lactams except monobactams, and the MBLs are not inhibited by clinically available serine-β-lactamase inhibitors. Two of the most commonly encountered MBLs in clinical isolates worldwide – the New Delhi metallo-β-lactamase (NDM-1) and the Verona integron-encoded metallo-β-lactamase (VIM-2) – are included in this study.

A series of several *N*H-1,2,3-triazoles was prepared by a three-step protocol utilizing Banert cascade reaction as the key step. The inhibitor properties were evaluated in biochemical assays against the MBLs VIM-2, NDM-1 and GIM-1, and VIM-2 showed IC_{50} values down to nanomolar range. High-resolution crystal structures of four inhibitors in complex with VIM-2 revealed hydrogen bonds from the triazole inhibitors to Arg228 and to the backbone of Ala231 or Asn233, along with hydrophobic interactions to Trp87, Phe61 and Tyr67. The inhibitors show reduced MIC in synergy assays with *Pseudomonas aeruginosa* and *Escherichia coli* strains harbouring VIM enzymes. The obtained results will be useful for further structural guided design of MBL inhibitors.

1. Introduction

The emergence and spread of antibiotic resistant bacteria are defined as a global health problem by the World Health Organization (WHO).[1] The increase in Gram-negative antibiotic resistant bacteria is particularly worrisome. Pan-resistance or extreme drug resistance are now commonly used terms to describe clinically important isolates of *Pseudomonas aeruginosa*, *Acinetobacter baumannii* and Enterobacteriaceae that are resistant to virtually all antibiotics.[2]

There are several causes for antibiotic resistance but the most common mechanism in gram negatives for β-lactam resistance, is the presence of β-lactamases enzymes that cleave the β-lactam ring rendering the drug inactive.[3–5] Drug treatment using β-lactamase inhibitors (BLI) as adjuvants to re-potentiate antibiotics is already in clinical use, e.g. the new serine-BLI avibactam has been approved in USA as a combination treatment with ceftazidime against complicated urinary tract infections and intra-abdominal infections.[5] Other examples in the clinic are the β-lactam-BLI combinations amoxicillin-clavulanate, ticarcillin-clavulanate, ampicillin-sulbactam, and piperacillin-tazobactam.[5,6] These BLIs inactivate primarily class A serine β-lactamase (SBL) enzymes, and avibactam also inhibits class C and some class D SBL enzymes.[5,6]

For class B metallo-β-lactamases (MBLs) no clinically approved BLIs are available. Lately, interesting results have been reported for the thiazole-4-carboxylic acid analogue ANT431 showing promising results against NDM-1 (K_i = 0.29 μM) and VIM-2 (K_i = 0.19 μM) including *in vivo* inhibitor efficacy.[7] Other recently described inhibitors include the natural product aspergillomarasmine,[8] which showed *in vivo* inhibitor efficacy against NDM-1, azolylthioacetamides[9] with K_i (NDM-1) = 0.43 μM, bisthiazolidines[10] with K_i (NDM-1) = 7–19 μM and 1,2,4-triazole-3-thiones with K_i (NDM-1) = 0.72 μM.[11,12] However, the clinical need for an MBL inhibitor is still outstanding.

Fokin and coworkers reported that 1,2,3-*N*H-triazoles of the general formula **1** were promising VIM-2 inhibitors.[13,14] In their study, the best compounds (**1cc'**and **1cd'**) showed sub-micromolar activity (IC_{50} = 0.07 μM; K_i = 0.02 μM) against VIM-2, and were able to re-potentiate the β-lactam antibiotic imipenem in VIM-2 producing *Escherichia coli* (BL21) cells when tested at 150 μM concentration.[13] Based

Abbreviations: DMSO, dimethyl sufoxide; GIM, German imipenemase; IC_{50}, half maximal inhibitory concentration; IPM, imipenem; MBL, metallo-β-lactamase; NCF, nitrocefin; NDM, New Delhi metallo-β-lactamase; VIM-2, Verona integron-encoded metallo-β-lactamase

* Corresponding authors.
E-mail addresses: annette.bayer@uit.no (A. Bayer), hanna-kirsti.leiros@uit.no (H.-K.S. Leiros).

https://doi.org/10.1016/j.bmc.2020.115598
Received 8 January 2020; Received in revised form 26 May 2020; Accepted 9 June 2020
Available online 18 June 2020

on docking studies, they predicted **1** to bind to the VIM-2 active site through the sulfonyl group as a zinc binding group. We became interested in gaining insight into the inhibitory action of the 1,2,3-*N*H-triazoles **1** in order to further explore the potential of this scaffold as MBL inhibitors. With our experience in crystallization of inhibitors with MBLs,[15–17] we aimed for crystallographic studies of enzyme–inhibitor complexes to understand the mode of binding and low IC_{50} values exhibited by the 1,2,3-*N*H-triazoles **1**. The exact interactions involved in the substrate binding of VIM- 2 are not clear, since no crystal structure in complex with a substrate has been reported.

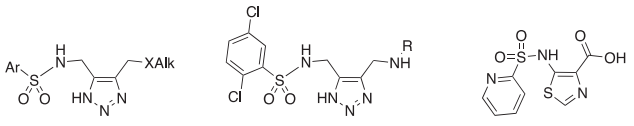

Here, we report the synthesis of a small focussed library of new and reported[13,14] (**1cc'**, **1cd'**, **1dg'**, **1dh'**) analogues of 1,2,3-*N*H-triazoles and our investigation of their potential as inhibitors of the previously reported VIM-2, and additionally NDM-1, a clinically important MBL, and GIM-1. The compounds were evaluated in biochemical and cell-based assays, and for the most promising compounds the inhibitory effect in synergy with meropenem was tested against clinical strains of *P. aeruginosa* (VIM-2), *K. pneumoniae* (NDM-1) and *E. coli* (VIM-29). We obtained crystal structures of four inhibitors in complex with VIM-2. In addition, a structure activity relationship (SAR) analysis of the observed inhibition patterns is provided using reported crystal structures of the three target enzymes (NDM-1 complex with hydrolysed ampicillin[18], VIM-2 in complex with fragments [17] and wild type GIM-1 [19]).

2. Results and discussion

2.1. Synthesis of NH-1,2,3-triazole inhibitors

A small library of *N*H-1,2,3-triazoles **1aa'–1dj'** were synthesized as shown in Scheme 1A.[13] Treatment of 4-chlorobutyneamine **2** with sulfonyl chlorides and base (K_2CO_3) provided the chlorosulfonamides **3a-d**, which were converted to the respective azidosulfonamides **4a-d**. The crude azides **4a–d** containing different sulphonamide groups (R^1 in red) underwent the Banert cascade[20–22] to *N*H-triazole sulphonamides **1aa'-di'** in the presence of a range of nucleophiles (R^2 in blue). For a mechanistic proposal of the Banert cascade see Scheme 1B.[21,23,24] The acetate substituted triazole **1dj'** was prepared by acetylation of the corresponding alcohol obtained from cyclisation with water as nucleophile.

2.2. Characterization of inhibitor properties against VIM-2, GIM-1 and NDM-1

The inhibitory activities of the *N*H-1,2,3-triazoles **1aa'–1dj'** against the MBLs VIM-2, GIM-1 and NDM-1 were evaluated as the half maximal inhibitory concentration (IC_{50}) values in biochemical competition assays (Table 1). For VIM-2 and GIM-1, the IC_{50} values were measured using nitrocefin as a reporter substrate, while IC_{50} values for NDM-1 were measured with imipenem as reporter substrate. Nitrocefin is hydrolysed by NDM-1 with a too high catalytic efficiency and is unsuitable as a reporter substrate for NDM-1.[25] The sequence identity between the three MBL enzymes used is 28% for VIM-2 versus GIM-1, 32% between VIM-2 and NDM-1 and 24% between NDM-1 and GIM-1.[15]

Compounds **1cc'**, **1cd'**, **1dg'** and **1dh'** have been evaluated as VIM-2 inhibitors by Fokin and coworkers resulting in IC_{50} values of 0.07 μM for **1cc'**, **1cd'** and **1dh'** and 7.3 μM for **1dg'**,[13] which were similar to our IC_{50} values of 0.23 (**1cc'**), 0.12 (**1cd'**), 0.53 (**1dh'**) and 15 (**1dg'**) μM (Table 1). When these triazoles were investigated against GIM-1, the inhibition was poor for **1dg'** (IC_{50} = 169 μM) and **1dh'** (IC_{50} = 193 μM) and no inhibition was observed for **1cc'** and **1cd'** and none of the four triazoles (**1cc'**, **1cd'**, **1dg'** and **1dh'**) were active against NDM-1.

Investigation of an extended library containing triazoles **1aa'-dj'** confirmed the observation that the compounds with the general structure of **1** were selective VIM-2 inhibitors with IC_{50}s ranging from 0.07 to 23 μM, while inhibition of GIM-1 and NDM-1 was generally weaker. GIM-1 was inhibited by 9 compounds (IC_{50}s from 18 to 353 μM) with **1dd'** (IC_{50} = 18 μM) being the best inhibitor. The reason for the weak inhibition of GIM-1 is not obvious and other inhibitor classes showed good inhibition towards GIM-1 in this assay.[15] Only 7 compounds were active against NDM-1 (IC_{50}s from 81 to 231 μM) with **1de'**

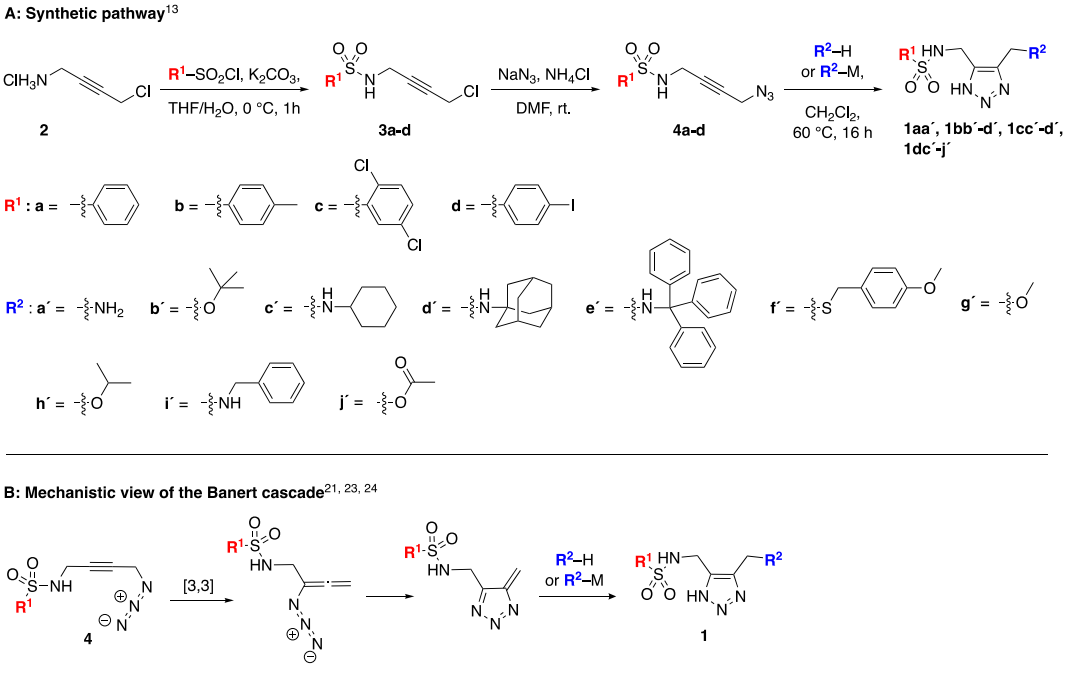

Scheme 1. Synthesis and structures of *N*H-1,2,3-triazole based inhibitors.

Table 1
The molecular structures of the synthesized inhibitors with measured inhibition concentrations (IC_{50}) against pure VIM-2, GIM-1 and NDM-1 enzymes; followed by % inhibition (equation 1) in *E. coli* SNO3 bacterial whole cell experiments with bla_{VIM-2}, bla_{GIM-1} or bla_{NDM-1}.

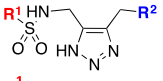

		VIM-2		GIM-1		NDM-1	
R^1	R^2	IC_{50} (μM)[a]	% inhib[a]	IC_{50} (μM)[a]	% inhib[a]	IC_{50} (μM)[b]	% inhib[b]
1aa'		23	29	NI	NI	NI	NI
1bb'	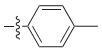	7.2	60	128	4.5	142	NI
1bc'		1.5	82	NI	2.3	144	NI
1bd'	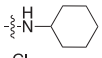	2.3	84	83 (67)	NI	ND	NI
1cc'*	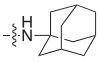 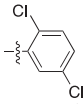	0.23	94	NI	7	98	NI
1cd'	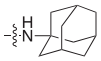	0.12	NI	P (7.7)	21	ND	NI
1dc'	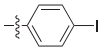 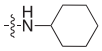	0.067	95	69	3	148	NI
1dd'	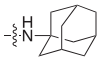	0.16	96	18	22	ND	17
1de'	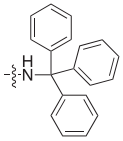	> 250	19	353	3	81	NI
1df'	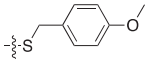	21	45	227	33	ND	34
1dg'		15	51	169	11	NI	NI
1dh'*		0.53	85	193	11	NI	NI
1di'*	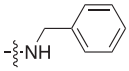	P	ND	ND	ND	ND	ND
1dj'*		23	ND	48	ND	231	ND

[a]The reported substrate was nitrocefin; [b]the reported substrate was imipenem; NI: no observable inhibition; ND: not determined; P: precipitated. *A VIM-2 complex structure is reported here.

(IC_{50} = 81 μM) being the most active compound.

The most potent VIM-2 inhibitors **1cc'** and **1cd'** (R^1 = 2,5-dichlorophenyl and **1dc'** and **1dd'** (R^1 = 4-iodophenyl) showed high nanomolar inhibition (IC_{50} = 0.067–0.23 μM). These compounds are structurally similar as they contain halogenated aromatic R^1 substituents although with different spatial arrangement (2,5-substitution compared to 4-substitution) and cyclic alkyl amino groups as R^2 substituents (cyclohexyl or adamantly), which may explain the similar inhibition properties.

The library contained two series of compounds containing identical R^2 groups; one consisting of **1bc'** (IC_{50} = 1.5 μM), **1cc'** (IC_{50} = 0.23 μM) and **1dc'** (IC_{50} = 0.067 μM) with R^2 like cyclohexylamino and the other consisting of **1bd'** (IC_{50} = 2.3 μM), **1cd'** (IC_{50} = 0.12 μM), and **1dd'** (IC_{50} = 0.16 μM) with R^2 like adamantylamino. Comparison of the compounds in a series provided an indication that the halogenated R^1 groups of compounds **1cc'**/**1cd'** (R^1 = 2,5-dichlorophenyl) and **1dc'**/**1dd'** (R^1 = 4-iodophenyl) were slightly advantageous (a 5–10-fold reduction in IC_{50}s) over the hydrocarbon based R^1 group of compounds **1bc'**/**1bd'** (R^1 = 4-methylphenyl).

A wide range of R^2 substituents were investigated in the **1d** series (Table 1). The inhibition of VIM-2 varied from IC_{50} of 0.07 μM for **1dc'** (R^2 = cyclohexylamino) to IC_{50} > 250 μM for **1de'** with the very bulky triphenylmethylamino group as R^2 substituent. In the middle range (IC_{50} = 15–21 μM), we found inhibitors **1df'** (R^2 = 4-methoxybenzylsulfide), **1dg'** (R^2 = isopropoxy) and **1dj'** (R^2 = acetate) with structurally very different R^2 substituents. Unfortunately, inhibitor **1di'** with benzylamine as R^2 substituent resulted in precipitation.

2.3. Evaluation of inhibitors in bacterial cell assays, with whole E. coli cells and synergy assays

To investigate the inhibitory activity against MBLs in bacterial cells, two different assays were used. The first was *E. coli* SNO3 cells transformed with bla_{VIM-2}, bla_{GIM-1} or bla_{NDM-1} (Table 1). The enzyme production was induced by addition of IPTG. The inhibitory activity was measured as the difference in speed of hydrolysis of the reporter substrate between the presence and absence of inhibitor, according to equation 1. A high degree of inhibition then indicate that the inhibitor prevents the MBL hydrolytic activity of breaking down the reporter substrate, and works as an inhibitor in a cell.

The inhibitory activities against VIM-2 in bacterial cells of **1aa'**-**1dj'** (Table 1) varied from 95% inhibition to inactive and were in good agreement with the inhibition determined in the biochemical assay. The

most active inhibitors (**1bb'**, **1bc'**, **1cc'**, **1cd'**, **1dc'** and **1dd'**) determined in the biochemical assay (IC_{50} from 0.07 to 2.3 μM) gave 82–96% inhibition in the cell based assay, except for **1cd'**, where no inhibition was found in the whole cell assay. This indicates that the inhibitors cross the outer *E. coli* membrane and hit VIM-2 localized in the periplasmic space. The reason for **1cd'** only being active towards purified VIM-2 (IC_{50} = 0.12 μM) and not in the whole cell assay (with VIM-2), can be that this inhibitor did not cross the outer *E. coli* membrane thus different from the most active inhibitors.

For GIM-1 producing *E. coli* SNO3 cells, we observed much lower levels of percent inhibition for inhibitors **1aa'**-**1dj'** with 3–25% in agreement with the higher IC_{50} values observed against this enzyme compared to VIM-2 (Table 1). The highest percent inhibition was obtained for **1df'** with 33%. In the NDM-1 whole cell assay, the percent inhibition was further decreased with most of the investigated compounds showing no inhibition (Table 1). Only inhibitors **1dd'** and **1df'** showed inhibitor properties with 17% and 34% inhibition, respectively.

Additionally a second cell based assay was performed where the inhibitory effect in synergy with meropenem of **1cc', 1dd'**, **1dc'**, **1dh'**, **1di'** and **1dj'** was tested against clinical strains of *P. aeruginosa* (VIM-2), *K. pneumoniae* (NDM-1) and *E. coli* (VIM-29) (Table 2). Not surprising, none of the tested inhibitors affected the NDM-1 producing *K. pneumoniae* strain. Inhibitor **1cc'** gave a reduced MIC from 64 to 8 mg/L in VIM-2 producing *P. aeruginosa*, but did not affect the *E. coli* strain. Our most promising hit is **1dj'**, which at low inhibitor concentration (50 mM) lowered the MIC from 64 to 1 mg/L for VIM-2 producing *P. aeruginosa* and from 16 to 1 mg/L for VIM-29 producing *E. coli*. VIM-2 and VIM-29 have 90% sequence identity, thus it is likely that an *E. coli* producing VIM-29 could also be inhibited and give a reduce MIC. In the synergy assay meropenem was the reporter substrate. The own effect from the inhibitors (> 500 μM) did not show any toxicity (data not shown).

2.4. Triazole inhibitors bound to VIM-2 in crystal structure complexes

Crystal structures of VIM-2 in complex with the inhibitors **1cc', 1dh', 1di'** and **1dj'** were used to investigate the interactions involved in the binding of the inhibitors. For the inhibitors **1cc'**, **1dh'** and **1di',** the DMSO-free co-crystallization method[16] was applied to obtain complex structures, whereas the inhibitor **1dj'** was soaked into native VIM-2 crystals.

The complex structures with the inhibitors **1cc'** and **1dh'** crystallized in the space group $P2_12_12$ with one protein molecule in the asymmetric unit. The two other complexes structures crystallized in the space group C2 with two protein molecules in the asymmetric unit. Space group C2 has previously been reported for VIM-2,[17] but space group $P2_12_12$ has not been observed before. The resolution of the obtained structures was ≤1.5 Å, with the complex structure VIM-2_**1cc'** showing the best resolution of 1.07 Å. To our knowledge, this is the highest resolution structure so far reported for VIM-2. Details on the statistics for the data collection and the refinement are shown in Table 3 and Table 4.

Table 2
Synergy test of selected inhibitors against clinical strains containing VIM-2, NDM-1 or VIM-29 and meropenem (MEM) or MEM and inhibitor to determine the MIC in mg/L. The inhibitor concentrations were 50 μM **(1cc', 1dh'**, **1di'**, **1dj')** or 125 μM (**1dd'**, **1dc'**).

Ref. no	K34-7	K66-45	50639799
Species	*P. aeruginosa*	*K. pneumoniae*	*E. coli*
MBL	VIM-2	NDM-1	VIM-29
	MIC (mg/L)	MIC (mg/L)	MIC (mg/L)
MEM	64	32–64	16
MEM + 1cc'*	8	32	16
MEM + 1dd'	16	32	nd
MEM + 1dc'	8	64	nd
MEM + 1dh'*	P	P	P
MEM + 1di'*	P	P	P
MEM + 1dj'*	1	64	1

* a VIM-2 complex structure is reported here. nd: not determined.
P: precipitated

Overall the protein structures as well as active site conformations of the obtained VIM-2 complexes were all in accordance with previously reported structures and no major differences were noticed. [15–17,26–28] The crystal structures with the inhibitors **1dh'** and **1cc'** showed unassigned electron density in the active site of the enzyme, clearly corresponding to the inhibitors (Fig. 1**A and D**). Also, the structures with inhibitors **1di'** and **1dj'** showed unassigned electron density in the active site of one or both VIM-2 protein molecules, respectively. However, this electron density was less well defined and more ambitious to interpret, reflecting a lower occupancy and a higher degree of disorder of the bound inhibitors (Fig. 1**G** and **K**). Several of the structures showed radiation damages,[29–31] caused to interactions between the bright synchrotron X-ray beam and the protein in the crystal. This is seen as positive peaks in the difference Fourier electron density maps. Upon radiation damage, the absorbed energy is dissipated as covalent bond breakage and heat resulting in higher thermal vibration. In the complex structure with the inhibitor **1dh'** and **1cc'**, the Cys221 was partially oxidized to the cysteine sulfonate, a radiation damage previously observed for VIM-2.[17,28] Furthermore, radiation damage in the iodine-carbon bound in the inhibitors **1dh', 1di'** and **1dj'** was observed, most likely due to electron capture. [30]

The position of the four inhibitors in the active site of VIM-2 and the interactions with the protein are shown in Fig. 1. A common feature in the binding mode of all inhibitors was the orientation of the *N*H-1,2,3-triazole moiety and the sulfonamide group. The triazole moiety directly interacted with one of the two zinc ions in the active site (Zn2) and with the bridging hydroxide ion. In addition, one of the nitrogen atoms in the triazole ring formed an interaction with Arg228 through a hydrogen bond. The sulfonamide group occupied slightly different positions in the complex structures of **1cc'**, **1dh'**, **1di'** and **1dj'** (conformation A). However, the main orientation was similar and allowed hydrogen bond interactions with the protein backbone of Ala231 and/or Asn233. Previously reported docking studies with arylsulfonamid-*N*H-123-triazoles suggested that either the sulfonamide group[13,14] or the triazole ring[32] interact with the zinc ions in the active site. Furthermore, in all docking studies the hydroxide ion bridging the two zinc ions was replaced by the inhibitor. In contrast, our results clearly show that the hydroxide ion is not replaced by the inhibitors and that the triazole moiety interacts only with one of the two zinc ions (Zn2), whereas the sulfonamide group does not participate in the zinc binding.

The inhibitors **1dh', 1di'** and **1dj'** have a 4-iodophenyl group in the R^2 position towards His263 and Arg228. In all structural complexes with these inhibitors, the iodine-carbon bond was radiation damaged and the electron density map clearly showed that the iodine was separated from the inhibitor (Fig. 1**D, G** and **K**). These radiation damages most likely induced changes in the orientation of the benzene ring as well as the iodine, as also observed for a brominated DNA/RNA hybrid.[30] Hence, the interpretation of the interactions with the iodophenyl group was difficult. However, the results indicate that the moiety forms hydrophobic interaction with Tyr67 and His263. Furthermore, the benzene ring might form a cation-π stacking with Arg228. In the inhibitor **1cc'**, the iodobenzene moiety in position R^2 is replaced by a dichlorobenzene, which adopts two different conformation. In both conformations, the benzene ring forms hydrophobic interactions with the Tyr67, with conformation A adopting an orientation better suited for a π - π stacking. In addition, one of the chlorine ions interacts in both conformations with Arg228 and in conformation B with the backbone of Ala231.

All four inhibitors have different substituents in the R^1 position towards Trp87. The inhibitor **1cc'** has a cyclohexylamine moiety at this position. The cyclohexyl ring of the moiety interacts with His118,

Table 3
X-ray data collection statistics for VIM-2 in complex with compound **1cc'**, **1dh'**, **1di'** and **1dj'**. Values in parenthesis are for the highest resolution shell.

	VIM-2_**1cc'**	VIM-2_**1dh'**	VIM-2_**1di'**	VIM-2_**1dj'**
Diffraction source	ID23-1, ESRF	ID23-1, ESRF	ID29, ESRF	ID29, ESRF
Wavelength (Å)	0.97625	0.97625	0.983998	0.983998
Temperature (°C)	−173	−173	−173	−173
Crystal-detector distance (mm)	158.67	201.24	275.00	275.00
Rotation range per image (°)	0.15	0.1	0.05	0.1
Total rotation range (°)	135	130	130	180
Exposure time per image (s)	0.037	0.037	0.04	0.037
Space group	P 2_12_12	P 2_122_1	C2	C2
a, *b*, *c* (Å)	98.35, 44.34, 60.84	90.75, 45.81, 63.93	100.59, 79.03, 67.24	101.28, 79.27, 67.69
γ (°)	90.00	90.00	130.09	130.35
Resolution range (Å)	38.26–1.07 (1.10–1.07)	52.26–1.40 (1.43–1.40)	31.33–1.50 (1.52–1.50)	39.63–1.50 (1.52–1.50)
No. of unique reflections	115,206	52,181	61,683	64,863
Multiplicity	4.8 (4.5)	4.7 (4.6)	2.5 (2.5)	3.4 (3.3)
Completeness (%)	97.8 (93.6)	98.3 (87.4)	95.8 (98.0)	99.5 (1 0 0)
R_{merge} (%)	6.4 (100)	6.3 (10.5)	4.8 (27.9)	7.2 (87.9)
Mean $\langle I/\sigma_{(I)}\rangle$	11.4 (1.5)	13.0 (1.5)	11.5 (2.7)	9.4 (1.2)
Overall *B*-factor from Wilson plot (Å^2)	10.41	17.31	13.60	16.38

Table 4
Crystallographic refinement statistics for VIM-2 in complex with compounds **1cc'**, **1dh'**, **1di'** and **1dj'**.

	VIM-2_**1cc'**	VIM-2_**1dh'**	VIM-2_**1di'**	VIM-2_**1dj'**
PDB entry	6TM9	6TMC	6TMB	6TMA
Final R_{work} (%)	11.01	13.16	13.87	15.74
Final R_{free} (%)	12.50	15.80	16.42	19.54
Molecules in asymmetric unit	1	1	2	2
No. of non-H atoms				
Protein	1989	1888	3676	3600
Ions	2 Zn^{2+}, 1 Cl^-, 1 OH^-	2 Zn^{2+}, 1 Cl^-, 1 OH^-	6 Zn^{2+}, 4 Cl^-, 2 OH^-	6 Zn^{2+}, 4 Cl^-, 2 OH^-
Ligand	52 (2 conformations)	23	26	86 (2 conformations)
Water	526	344	662	627
R.m.s. deviations				
Bonds (Å)	0.010	0.012	0.010	0.005
Angles (°)	1.217	1.005	1.016	0.748
Average *B* factors (Å^2)				
Protein	13.87	20.9	17.32	22.72
Ion	10.94	17.3	21.80	27.94
Ligand (occupancy)	14.56 (0.6/0.3)	22.9 (0.86)	46.61 (0.78)	64.31 (0.51/0.49)
Water	33.16	38.6	34.46	37.53
Ramachandran plot				
Most favoured (%)	97.12	96.9	97.75	97.93
Allowed (%)	2.06	2.2	2.25	1.61

Trp87 and Phe61, and the amine nitrogen interacts with the hydroxide ion located between the two active site Zn ions (Fig. 1**B, C**) through a hydrogen bond. Similar interactions were observed both for inhibitor **1dh'** between the catalytic hydroxide ion and the oxygen of the isopropoxy moiety (Fig. 1**E, F**) and for inhibitor **1di'** involving the nitrogen of the benzylamino group (Fig. 1**H, I**). In the latter complex structure, the benzene ring of the benzylamino group additionally seems to interact with Trp87, Phe61 and Tyr67. However, for the benzylamino group of **1di'** and the methyl acetate moiety of **1dj'**, only weak electron densities were observed. Hence, the interpretation of the exact orientations and the interactions with the protein were difficult. The weak electron density and the disordered structure might indicate that these moieties do not form strong interactions with the protein.

The binding interactions identified in the above VIM-2 inhibitor complexes may explain the reduced inhibitor activity of the NH-triazoles towards NDM-1 and GIM-1. The important residue determinants in the NDM-1 binding site are Phe63, Lys224 and Ala228 (see e.g. [15]). In the VIM-2 inhibitor complexes, we observed hydrophobic interactions with Tyr67 and cation - π stacking interactions with Arg228, which both are not possible with the corresponding Val67 and Ala228 in NDM-1. On the other hand, the hydrogen bonding interaction of the NH-triazole to Arg228 in VIM-2 may be possible with the adjacent Lys224 in NDM-1. The GIM-1 the binding site includes Tyr64, Val67, Arg224 and Trp228. For GIM-1, the guanidino group of Arg224 overlaps with the corresponding group of Arg228 in VIM-2 making hydrogen bonding to the *N*H-triazole possible. However, Tyr64 in GIM-1 is too far away to replace the nice π - π stacking involving Tyr67 in VIM-2, thus might explain the lower inhibitor potential with high IC_{50} values for GIM-1. Moreover, VIM-29 (UniProt J7HGI2), present in the *E. coli* strain used for the synergy assay, carries Tyr67, His224 and Ser228, so the polar His224 and aromatic Tyr67 could allow for good inhibitor binding and support the low MIC in the synergy assays (Table 2).

3. Conclusion

Inspired by encouraging results on using triazoles as MBL inhibitors, we prepared a small focused chemical library with 15 *N*H-1,2,3-triazole molecules, which was tested for inhibitory against VIM-2, GIM-1 and NDM-1.

We found that VIM-2 was inhibited by several *N*H-1,2,3-triazole and the new inhibitor **1dc'** gave nano-molar affinity with IC_{50} of 0.067 μM. This inhibitor also affected GIM-1 (IC_{50} = 69 μM) and NDM-1 (IC_{50} = 148 μM), but to a much lower extent.

The most promising inhibitor was **1dj'** with moderate IC_{50} values of 23 μM (VIM-2), 48 μM (GIM-1) and 231 μM (NDM-1). More interestingly, the synergy assay found **1dj'** to effects two clinical isolates. One

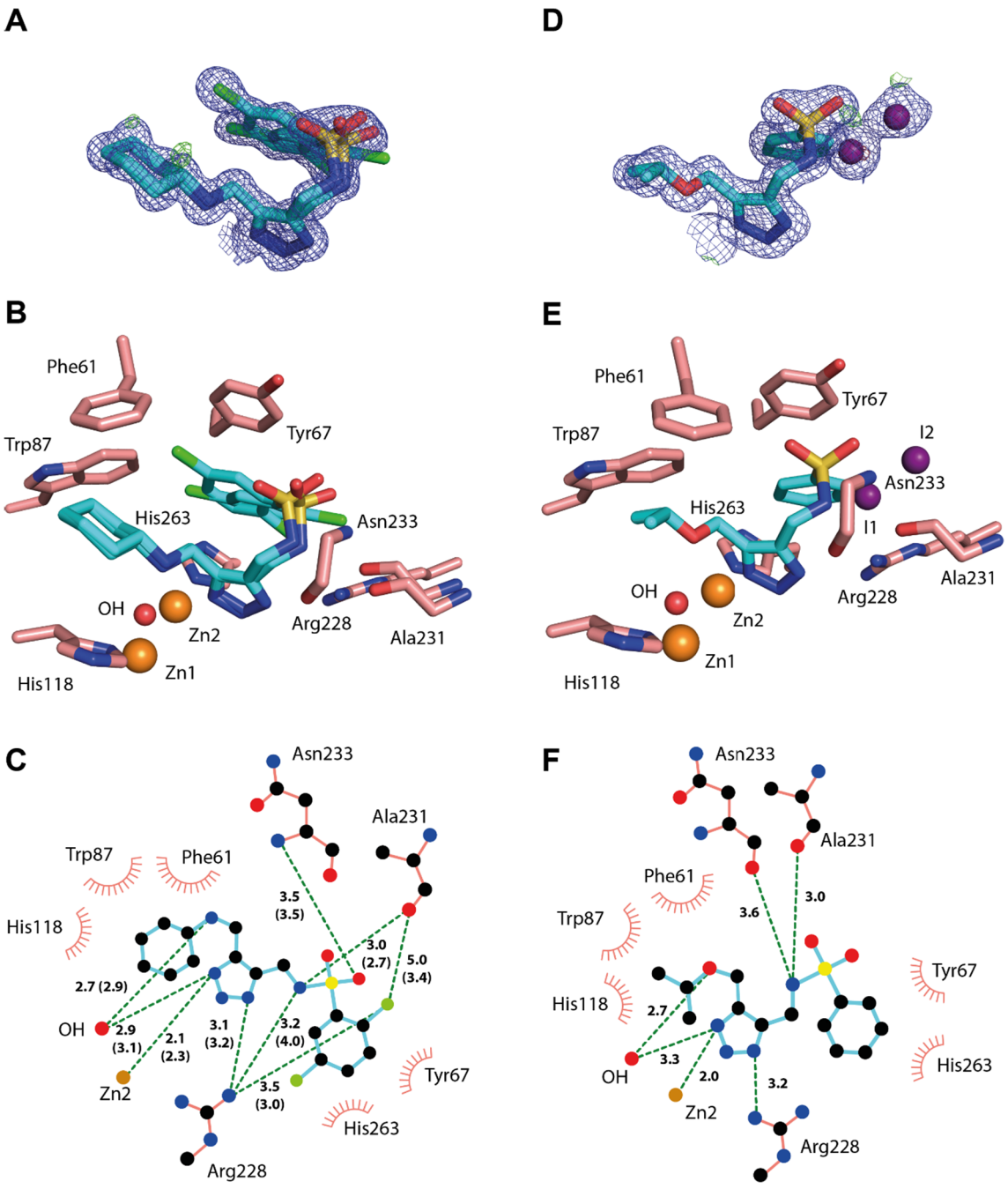

Fig. 1. Final elections density maps (A, D, G and K), crystal structures (B, E, H and L) and interaction plots (C, F, I and M) for the inhibitor **1cc'** (A, B and C), **1dh'** (D, E, and F), **1di'** (G, H and I) and **1dj'** (K, L and M). The $2F_0$-F_C maps are shown in blue at 1.0σ for **1cc'** and **1dh'** and at 0.9σ for **1di'** and **1dj'**. The F_C-F_0 maps are shown at 4σ (green) and −4σ (red). In the crystal structures, carbon atoms of the inhibitors are depicted in cyan and protein carbon atoms in salmon. For the interaction plots, crystal structures were analysed using LIGPLOT.[33] Hydrogen bonds are shown as green dashed lines and hydrophobic interactions by red arcs. All distances are given in Å. Distances for alternative conformation are given in brackets. For inhibitor **1dj'**, the figures are only shown for the VIM-2 molecule with higher ligand occupancy. In panel G, two water molecules are shown (red sphere), which are assumed to be artefacts from the native structure without bound ligand.

P. aeruginosa producing VIM-2 reduced the MIC from 64 mg/L with only meropenem to only 1 mg/L for meropenem and **1dj'**; and an *E. coli* producing VIM-29 showed reduced MIC from 16 mg/L (only meropenem) to 1 mg/L when combining meropenem and **1dj'**. The 1.50 Å complex structure of VIM-2_**1dj'** show tight aromatic π - π stacking to Tyr67, binding from the *N*H-1,2,3-triazole group to Arg228 and the active site Zn2 ion, and the presence of the hydroxyl ion between the two zinc ions. Our new complex structure of VIM-2_**1dj'** is therefore a valuable starting point for structure guided inhibitor design of a new inhibitor targeting several MBL enzymes simultaneously.

4. Materials and methods

4.1. Organic synthesis

All reagents and solvents were purchased from commercial sources and used as supplied unless otherwise stated. Compounds **3a**, **3c**, **3d**, **4a**, **4c**, **4d**, **1cc'**, **1cd'**, **1dg'** and **1dh'** were prepared according to the literature.[13] Reactions were monitored by thin-layer chromatography (TLC) with Merck pre-coated silica gel plates (60 F_{254}). Visualization was accomplished with either UV light or by immersion in potassium

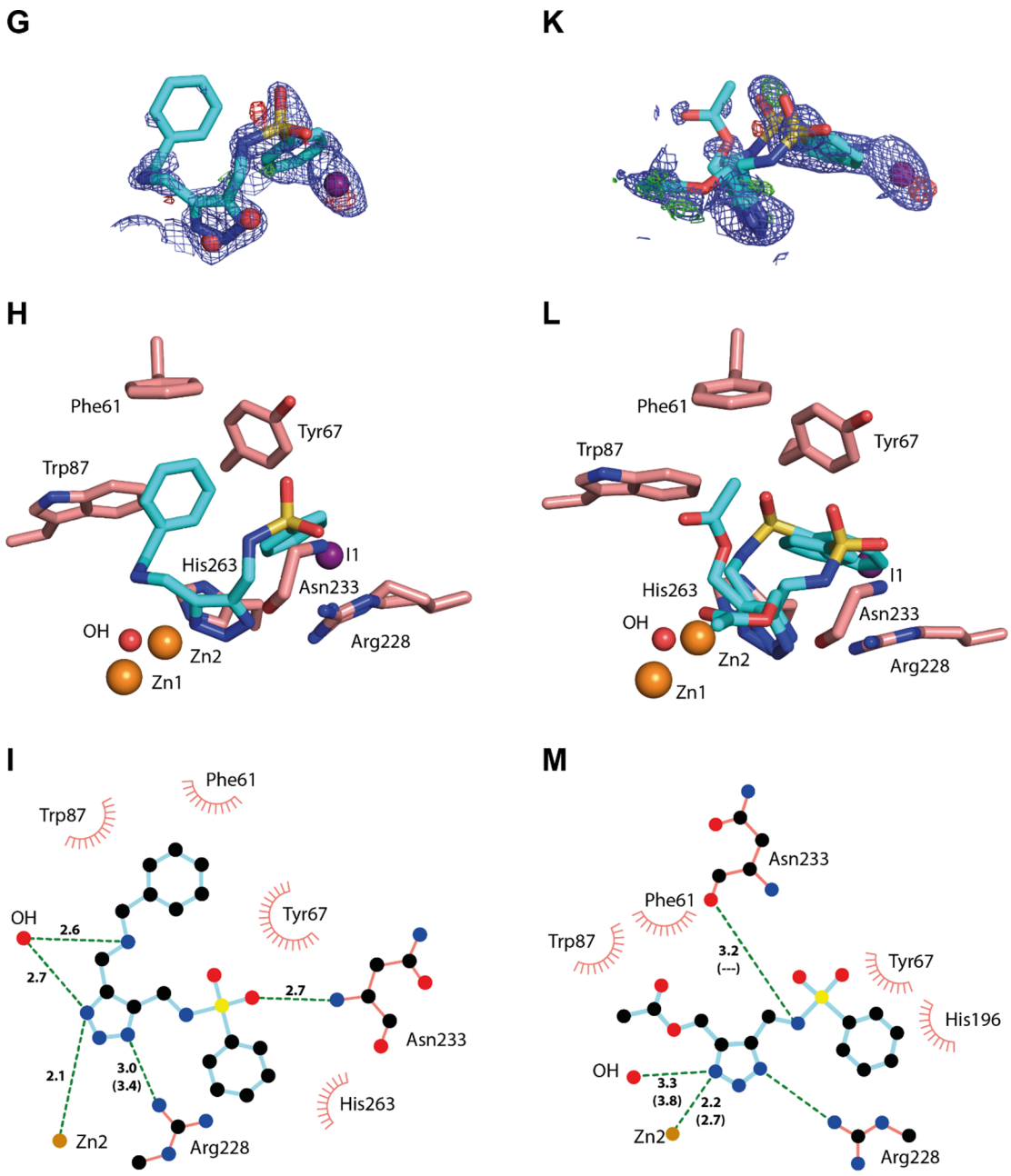

Fig. 1. (*continued*)

permanganate or phosphomolybdic acid (PMA) followed by light heating with a heating gun. Purification of reactions was carried out by flash column chromatography using silica gel from Merck (Silica gel 60, 0.040–0.063 mm). Purity analysis was carried out on Waters Acquity UPLC® BEH C18 (1.7 µm, 2.1 × 100 mm) column on a Waters Acquity I-class UPLC with Photodiode Array Detector. NMR spectra were obtained on a 400 MHz Bruker Avance III HD equipped with a 5 mm SmartProbe BB/1H (BB = 19F, 31P-15 N). Data are represented as follows: chemical shift, multiplicity (s = singlet, d = doublet, t = triplet, q = quartet, m = multiplet), coupling constant (J, Hz) and integration. Chemical shifts (δ) are reported in ppm relative to the residual solvent peak ($CDCl_3$: δ_H 7.26 and δ_C 77.16; Methanol-d_4: δ_H 3.31 and δ_C 49.00). Positive ion electrospray ionization mass spectrometry was conducted on a Thermo electron LTQ Orbitrap XL spectrometer.

4.1.1. Synthesis of the sulfonamide derivatives from the corresponding sulfonylchlorides

The sulfonamides were prepared following the a procedure described by Weide *et al.*[13]

4.1.1.1. N-(4-chlorobut-2-ynyl)benzenesulfonamide (3a)[13]. Benzenesulfonylchloride (500 mg, 2.8 mmol, 1.0 equiv), 4-chlorobut-2-yn-1-amine hydrochloride **2** (515.26 mg, 3.68 mmol, 1.3 equiv), and K_2CO_3 (1.161 g, 8.4 mmol, 3.0 equiv), in THF/H_2O (14 mL, 1:1) gave compound **3a** (650 mg, 72%) as a colorless solid. R_f = 0.37 (hexane/ethyl acetate, 65:35). Analytical data were in accordance with literature.[13] ^{1}H NMR (400 MHz, $CDCl_3$) δ 8.00 – 7.87 (m, 2H), 7.70 – 7.50 (m, 3H), 3.95 (t, J = 2.1 Hz, 2H), 3.89 (t, J = 2.1 Hz, 2H). ^{13}C NMR (101 MHz, $CDCl_3$) δ 139.4, 132.8, 128.9, 127.2, 80.3, 79.4, 77.2, 32.9, 29.6. HRMS (ESI): Calcd. for $C_{10}H_{10}O_2NClNaS$ $[M + H]^+$ 266.0012; found 266.0013.

4.1.1.2. N-(4-chlorobut-2-ynyl)-4-methylbenzenesulfonamide (3b). Toluene-4-sulfonylchloride (500 mg, 1.9 mmol, 1.0 equiv), 4-chlorobut-2-yn-1-amine hydrochloride **2** (477.42 mg, 2.50 mmol, 1.3 equiv), and K_2CO_3 (1.087 g, 7.5 mmol, 3.0 equiv), in THF/H_2O (12 mL, 1:1) gave compound **3c** (550 mg, 85%) as a colorless solid. R_f = 0.46 (hexane/ethyl acetate, 35:65). **^{1}H NMR** (400 MHz, $CDCl_3$): δ 7.77 (d, J = 8.3 Hz, 2H), 7.32 (d, J = 8.0 Hz, 2H), 3.88 (d, J = 2.1 Hz, 4H), 2.43 (s, 3H). **^{13}C NMR** (101 MHz, $CDCl_3$): δ 143.9, 136.6, 129.7, 129.5, 127.5, 80.7, 79.5, 33.1, 29.9, 29.4, 21.6. **HRMS (ESI)**: Calcd. for $C_{11}H_{12}O_2NClNaS$ $[M + H]^+$ 280.0169; found 280.0169.

4.1.1.3. 2,5-dichloro-N-(4-chlorobut-2-ynyl)benzenesulfonamide (3c)[13]. 2,5-Dichlorobenzenesulfonylchloride (1000 mg, 4.1 mmol, 1.0 equiv), 4-chlorobut-2-yn-1-amine hydrochloride **2** (741.4 mg, 5.3 mmol, 1.3 equiv), and K_2CO_3 (1.687 g, 12.21 mmol, 3.0 equiv), in THF/H_2O (21 mL, 1:1) gave compound **3d** (1.084 mg, 87%) as a colorless solid. R_f = 0.40 (hexane/ethyl acetate, 35:65). Analytical data were in accordance with literature.[13] **^{1}H NMR** (400 MHz, $CDCl_3$): δ 8.09 (d, J = 2.2 Hz, 1H), 7.52 – 7.48 (m, 2H), 5.33 (t, J = 6.5 Hz, 1H), 3.96 (d, J = 6.3 Hz, 2H), 3.82 (s, 2H). **^{13}C NMR** (101 MHz, $CDCl_3$): δ 138.6, 133.6, 133.3, 132.4, 130.9, 129.8, 79.7, 79.4, 77.2, 33.1, 29.3. **HRMS (ESI)**: Calcd. for $C_{10}H_8O_2NCl_3S$ $[M-H]^-$ 311.9233; found 311.9230.

4.1.1.4. 4-Iodo-N-(4-chlorobut-2-ynyl)-benzenesulfonamide (3d)[13]. 4-Iodobenzensulfonylchloride (1000 mg, 3.3 mmol, 1.0 equiv), 4-chlorobut-2-yn-1-amine hydrochloride **2** (602 mg, 4.3 mmol, 1.3 equiv), and K_2CO_3 (1.368 g, 9.9 mmol, 3.0 equiv), in THF/H_2O (18 mL, 1:1) gave compound **3e** (880 mg, 72%) as a colorless solid. R_f = 0.41 (hexane/ethyl acetate, 35:65). **^{1}H NMR** (400 MHz, $CDCl_3$): δ 7.96 – 7.83 (m, 2H), 7.61 (d, J = 8.6 Hz, 2H), 4.67 (s, 1H), 4.01 – 3.76 (m, 4H). **^{13}C NMR** (101 MHz, $CDCl_3$): δ 176.2, 139.5, 138.4, 128.8, 100.5, 80.3, 79.8, 33.1, 29.7. **HRMS (ESI)**: Calcd. for $C_{10}H_8O_2NClIS$ $[M-H]^-$ 367.9022; found 367.9003.

4.1.2. Synthesis of the azide derivatives from the corresponding chlorides

The azides were prepared following modified procedure based on Weide *et al.*[13]

4.1.2.1. N-(4-azidobut-2-ynyl)benzenesulfonamide (4a). *N*-(4-chlorobut-2-ynyl)benzenesulfonamide (**3a**) (100 mg, 0.41 mmol, 1.0 equiv), sodium azide (31.98 mg, 0.492 mmol, 1.2 equiv), and NH_4Cl (5.5 mg, 0.1 mmol, 0.25 equiv), in DMF (5 mL) gave compound **4a** (66.3 mg, 66%) as a colorless solid. R_f = 0.33 (hexane/ethyl acetate, 65:35). **^{1}H NMR** (400 MHz, $CDCl_3$): δ 7.91 (d, J = 7.0 Hz, 2H), 7.66 – 7.46 (m, 3H), 5.12 (s, 1H), 3.92 (s, 2H), 3.64 (s, 2H). **^{13}C NMR** (101 MHz, $CDCl_3$): δ 139.5, 132.7, 128.9, 127.1, 81.2, 76.9, 39.4, 32.8. **HRMS (ESI)**: Calcd. for $C_{10}H_{10}O_2N4NaS$ $[M + Na]^+$ 273.0419; found 273.0417.

4.1.2.2. N-(4-azidobut-2-ynyl)-4-methylbenzenesulfonamide (4b). *N*-(4-chlorobut-2-ynyl)-4-methylbenzenesulfonamide (**3b**) (100 mg, 0.39 mmol, 1.0 equiv), sodium azide (30.0 mg, 0.47 mmol, 1.2 equiv), and NH_4Cl (5.2 mg, 0.09 mmol, 0.25 equiv), in DMF (5 mL) gave compound **4b** (80 mg, 84%) as a colorless solid. R_f = 0.43 (hexane/ethyl acetate, 65:35). **^{1}H NMR** (400 MHz, $CDCl_3$): δ 7.78 (d, J = 8.3 Hz, 2H), 7.31 (d, J = 8.0 Hz, 2H), 5.03 (t, J = 5.8 Hz, 1H), 3.89 (d, J = 6.1 Hz, 2H), 3.67 (s, 2H), 2.42 (s, 3H). **^{13}C NMR** (101 MHz, $CDCl_3$): δ 144.3, 137.0, 130.1, 127.8, 82.0, 77.4, 40.1, 33.4, 21.9. **HRMS (ESI)**: Calcd. for $C_{11}H_{12}O_2N_4NaS$ $[M + Na]^+$ 287.0576; found 287.0573.

4.1.2.3. N-(4-azidobut-2-ynyl)-2,5-dichlorobenzenesulfonamide (4c). 2,5-Dichloro-*N*-(4-chlorobut-2-ynyl)benzenesulfonamide **3c** (1000 mg, 3.2 mmol, 1.0 equiv), sodium azide (250.8 mg, 3.85 mmol, 1.2 equiv), and NH_4Cl (42.4 mg, 0.8 mmol, 0.25 equiv), in DMF (49 mL) gave compound **4c** (980 mg, 96%) was obtained as a colorless solid. R_f = 0.41 (hexane/ethyl acetate, 65:35). **^{1}H NMR** (400 MHz, $CDCl_3$): δ 8.09 (d, J = 2.2 Hz, 1H), 7.48 (s, 2H), 5.43 (t, J = 6.2 Hz, 1H), 3.97 (dd, J = 6.3, 0.7 Hz, 2H), 3.63 (t, J = 2.0 Hz, 2H). **^{13}C NMR** (101 MHz, $CDCl_3$): δ 138.9, 133.92, 133.90, 133.6, 132.6, 131.2, 130.1, 80.6, 77.5, 77.2, 39.6, 33.2. **HRMS (ESI)**: Calcd. for $C_{10}H_7N_4O_2Cl_2S$ $[M-H]^-$ 316.9670; found 316.9661.

4.1.2.4. N-(4-azidobut-2-ynyl)-4-iodobenzenesulfonamide (4d). *N*-(4-chlorobut-2-ynyl)-4-iodobenzenesulfonamide **3d** (850 mg, 2.3 mmol, 1.0 equiv), sodium azide (179.7 mg, 2.76 mmol, 1.2 equiv), and NH_4Cl (36.6 mg, 0.69 mmol, 0.25 equiv), in DMF (30 mL) gave compound **4d** (780 mg, 90%) was obtained as a colorless solid. R_f = 0.37 (hexane/ethyl acetate, 65:35). **^{1}H NMR** (400 MHz, $CDCl_3$): δ 7.88 (d, J = 8.5 Hz, 2H), 7.61 (d, J = 8.5 Hz, 2H), 5.19 (s, 1H), 3.92 (s, 2H), 3.68 (d, J = 2.0 Hz, 2H). **^{13}C NMR** (101 MHz, $CDCl_3$): δ 139.5, 138.46, 138.45, 138.4, 128.9, 128.8, 100.6, 81.3, 77.4, 77.2, 39.8, 33.1. **HRMS (ESI)**: Calcd. for $C_{10}H_9IN_4O_2S$ $[M-H]^-$ 374.9412; found 374.9407.

4.1.3. General procedure for the synthesis of NH-triazole-arylsulfonamides

To azide **4a–d** (1 equiv) as solution in CH_2Cl_2 or neat was added the nucleophile (1–5 equiv.). The reaction mixture was stirred at 60 °C for 16 h. The reaction was concentrated under reduced pressure to give the crude product. All triazoles were purified by flash column chromatography on silica gel (50–100% EtOAc in hexanes to 10% MeOH in EtOAc). Repeated column chromatography provided most compounds with purity greater than 90% as determined by HPLC.

4.1.3.1. N-((5-(aminomethyl)-1H-1,2,3-triazol-4-yl)methyl) benzenesulfonamide (1aa'). *N*-(4-azidobut-2-ynyl)benzenesulfonamide **4a** (68 mg, 0.27 mmol, 1.0 equiv) and ammonium hydroxide solution (28% NH_3 in H_2O, 2 mL) gave **1aa'** (47 mg, 65%) as a pale yellow oil. **^{1}H NMR** (400 MHz, DMSO-d_6): δ 7.79 (s, 2H), 7.71 – 7.38 (m, 3H), 4.06 (s, 2H), 3.70 (s, 2H). **^{13}C NMR** (101 MHz, DMSO-d_6): δ 143.3, 140.6, 139.2, 132.8, 129.5, 129.5, 126.9, 37.7, 35.6. **HRMS (ESI)**: Calcd. for $C_{10}H_{14}O_2N_5S$ $[M + H]^+$ 268.0862; found 268.0863. **HPLC purity**: 91%

4.1.3.2. N-((5-(tert-butoxymethyl)-1H-1,2,3-triazol-4-yl)methyl)-4-methylbenzenesulfonamide (1bb'). *N*-(4-azidobut-2-ynyl)-4-methylbenzenesulfonamide **4b** (66 mg, 0.25 mmol, 1.0 equiv) in CH_2Cl_2 (2 mL) and 2-methyl-2-propanol (74 mg, 1.0 mmol, 4.0 equiv) gave **1bb'** (55 mg, 65%) as colorless oil. **^{1}H NMR** (400 MHz, CD_3OD): δ 7.69 (d, J = 8.2 Hz, 2H), 7.34 (d, J = 8.2 Hz, 2H), 4.50 (s, 2H), 4.18 (s, 2H), 2.42 (s, 3H), 1.26 (s, 9H). **^{13}C NMR** (101 MHz, CD_3OD): δ 144.8, 144.2 (determined from HMBC), 143.8 (determined from HMBC), 138.5, 130.7, 128.2, 75.5, 56.2, 38.6, 27.7, 21.4. **HRMS (ESI)**: Calcd. for $C_{15}H_{22}O_3N_4NaS$ $[M + Na]^+$ 361.1300; found 361.1305. **HPLC purity**: 87%

4.1.3.3. N-((5-((cyclohexylamino)methyl)-1H-1,2,3-triazol-4-yl)methyl)-4-methylbenzenesulfonamide (1bc'). *N*-(4-azidobut-2-yny)-4-methylbenzenesulfonamide **4b** (78 mg, 0.29 mmol, 1.0 equiv) and cyclohexylamine (115 mg, 1.16 mmol, 4.0 equiv) gave **1bc'** (75 mg, 71%) as colorless solid. **^{1}H NMR** (400 MHz, CD_3OD) δ 7.78 – 7.69 (m, 2H), 7.43 – 7.34 (m, 2H), 4.15 (s, 2H), 3.98 (s, 2H), 2.72 – 2.60 (m, 1H), 2.43 (s, 3H), 2.07 – 1.98 (m, 2H), 1.84 – 1.75 (m, 2H), 1.71 – 1.63 (m, 1H), 1.38 – 1.12 (m, 5H). **^{13}C NMR** (101 MHz, CD_3OD) δ 144.9, 140.9, 140.1, 138.4, 130.8, 128.2, 57.4, 40.3, 38.7, 32.6, 26.8, 25.9, 21.5. **HRMS (ESI)**: Calcd. for $C_{17}H_{26}O_2N_5S$ $[M + H]^+$ 364.1798; found 364.1802.

4.1.3.4. N-((5-((adamantylamino)methyl)-1H-1,2,3-triazol-4-yl)methyl)-4-methyl-benzenesulfonamide (1bd'). *N*-(4-azidobut-2-ynyl)-4-methylbenzenesulfonamide **4b** (20 mg, 0.07 mmol, 1.0 equiv) in CH_2Cl_2 (2 mL) and 1-

adamantylamine (34.2 mg, 0.226 mmol, 3.0 equiv) gave **1bd'** (24 mg, 83%) as colorless solid. **^{1}H NMR** (400 MHz, CD_3OD) δ 7.75 – 7.68 (m, 2H), 7.39 – 7.33 (m, 2H), 4.14 (s, 2H), 4.01 (s, 2H), 2.41 (s, 3H), 2.17 – 2.11 (m, 3H), 1.85 (d, J = 2.9 Hz, 6H), 1.79 – 1.66 (m, 6H). **^{13}C NMR** (101 MHz, CD_3OD) δ 144.9, 141.0, 139.5, 138.3, 130.8, 128.1, 55.6, 41.1, 38.7, 37.1, 35.2, 30.8, 21.5. **HRMS (ESI)**: Calcd. for $C_{21}H_{28}O_2N_5S$ $[M-H]^-$ 414.1970; found 414.1965. **HPLC purity**: 89%

*4.1.3.5. 2,5-Dichloro-N-((5-((cyclohexylamino)methyl)-1H-1,2,3-triazol-4-yl)methyl)benzenesulfonamide (**1cc'**)*[13]. *N*-(4-azidobut-2-ynyl)-2,5-dichlorobenzenesulfonamide **4c** (93 mg, 0.29 mmol, 1.0 equiv) in CH_2Cl_2 (4 mL) and cyclohexylamine (86.1 mg, 0.87 mmol, 3 equiv) gave **1 cc'** (88 mg, 72%) as colorless solid. **^{1}H NMR** (400 MHz, CD_3OD): δ 7.96 (d, J = 2.4 Hz, 1H), 7.57 (dd_{AB}, J = 8.5, 2.4 Hz, 1H), 7.53 (d_{AB}, J = 8.5 Hz, 1H), 4.27 (s, 2H), 3.99 (s, 2H), 2.74 – 2.62 (m, 1H), 2.05 – 2.02 (m, 2H), 1.82 – 1.78 (m, 2H), 1.69 – 1.65 (m, J = 12.5 Hz, 1H), 1.37 – 1.16 (m, 5H). **^{13}C NMR** (101 MHz, CD_3OD): δ 140.8, 140.7, 140.1, 134.6, 134.3, 134.1, 131.7, 131.3, 57.5, 40.2, 38.3, 32.6, 26.8, 25.9. **HRMS (ESI)**: Calcd. for $C_{16}H_{22}O_2N_5Cl_2S$ $[M + H]^+$ 418.0861; found 418.0866. **HPLC purity**: 95%

*4.1.3.6. 2,5-Dichloro-N-((5-((adamantylamino)methyl)-1H-1,2,3-triazol-4-yl)methyl)benzenesulfonamide (**1cd'**)*[13]. *N*-(4-azidobut-2-ynyl)-2,5-dichlorobenzenesulfonamide **4c** (102 mg, 0.32 mmol, 1.0 equiv), 1-adamentylamine (58.2 mg, 0.38 mmol, 1.2 equiv) in CH_2Cl_2 (4 mL) gave **1 cd'** (111 mg, 73%) as colorless solid. **^{1}H NMR** (400 MHz, CD_3OD) δ 8.00 – 7.95 (m, 1H), 7.62 – 7.51 (m, 2H), 4.28 (s, 2H), 3.97 (s, 2H), 2.16 (s, 3H), 1.86 (d, J = 2.9 Hz, 6H), 1.82 – 1.69 (m, 6H). **^{13}C NMR** (101 MHz, CD_3OD) δ 140.9, 140.6, 140.1, 134.6, 134.3, 134.2, 131.7, 131.3, 54.7, 41.6, 38.4, 37.3, 35.2, 30.9. **HRMS (ESI)**: Calcd. for $C_{20}H_{26}O_2N_5ClS$ $[M + H]^+$ 470.1182; found 470.1179. **HPLC purity**: 94%

N-((5-((cyclohexylamino)methyl)-1H-1,2,3-triazol-4-yl)methyl)-4-iodobenzenesulfonamide (1dc')

N-(4-azidobut-2-ynyl)-4-iodobenzenesulfonamide **4d** (86 mg, 0.228 mmol, 1.0 equiv), cyclohexylamine (83.9 mg, 0.845 mmol, 4.0 equiv) in CH_2Cl_2 (2 mL) gave **1dc'** (99 mg, 86%) as colorless oil. **^{1}H NMR** (400 MHz, $CDCl_3$): δ 7.82 (d, J = 8.1 Hz, 2H), 7.56 (d, J = 8.1 Hz, 2H), 4.08 (s, 2H), 3.99 (s, 2H), 2.80 (s, 1H), 2.13 – 2.01 (m, 2H), 1.76 (d, J = 7.1 Hz, 2H), 1.64 (d, J = 12.4 Hz, 1H), 1.34 – 1.11 (m, 6H). **^{13}C NMR** (101 MHz, $CDCl_3$): δ 139.9, 139.6, 138.3, 136.5, 128.5, 99.8, 57.5, 39.8, 38.4, 31.5, 25.5, 24.9. **HRMS (ESI)**: Calcd. for $C_{16}H_{23}O_2N_5SI$ $[M + H]^+$ 476.0612; found 476.0612. **HPLC purity**: 99%

*4.1.3.7. N-((5-((adamantylamino)methyl)-1H-1,2,3-triazol-4-yl) methyl)-4-iodobenzenesulfonamide (**1dd'**)*. *N*-(4-azidobut-2-ynyl)-4-iodobenzenesulfonamide **4d** (77 mg, 0.20 mmol, 1.0 equiv), 1-adamantylamine (37.2 mg, 0.226 mmol, 1.2 equiv) in CH_2Cl_2 (4 mL) gave **1dd'** (102 mg, 96%) as colorless solid. **^{1}H NMR** (400 MHz, DMSO-d_6): δ 8.01 – 7.89 (m, 2H), 7.55 – 7.50 (m, 2H), 5.78 – 5.73 (m, 1H), 4.14 – 4.05 (m, 2H), 3.70 – 3.63 (m, 2H), 3.23 – 3.12 (m, 1H), 2.00 (s, 3H), 1.65 – 1.48 (m, 12H). **^{13}C NMR** (101 MHz, DMSO-d_6): δ δ 142.2 (determined by HMBC), 139.9, 139.3 (determined by HMBC), 138.0, 128.3, 100.4, 50.4, 41.5, 37.6, 36.2, 34.2, 28.9. **HRMS (ESI)**: Calcd. for $C_{20}H_{27}O_2N_5SI$ $[M + H]^+$ 528.0925; found 528.0925. **HPLC purity**: 97%

*4.1.3.8. N-((5-((tritylamino)methyl)-1H-1,2,3-triazol-4-yl) methyl)-4-iodo-benzenesulfonamide (**1de'**)*. *N*-(4-azidobut-2-ynyl)-4-iodobenzenesulfonamide **4d** (100 mg, 0.26 mmol, 1.0 equiv) in CH_2Cl_2 (5 mL) and triphenylmethanamine (82.2 mg, 0.319 mmol, 1.2 equiv) gave **1de'** (63 mg, 93%) as colorless solid. **^{1}H NMR** (400 MHz, $CDCl_3$): δ 7.69 (d, J = 8.2 Hz, 2H), 7.43 (d, J = 8.1 Hz, 5H), 7.37 – 7.20 (m, 12H), 4.25 (s, 2H), 3.42 (s, 2H). **^{13}C NMR** (101 MHz, $CDCl_3$): δ 145.0, 139.6, 138.4, 128.7, 128.6, 128.31, 128.27, 128.1, 127.0, 100.1, 71.4, 38.4, 37.8. **HRMS (ESI)**: Calcd. for $C_{29}H_{26}O_2N_5SI$ $[M + Na]^+$ 658.0748; found 658.0744. **HPLC purity**: 81%

N-((5-((4-methoxybenzylthio)methyl)-1H-1,2,3-triazol-4-yl)methyl)-4-iodo-benzenesulfonamide (**1df'**)

N-(4-azidobut-2-ynyl)-4-iodobenzenesulfonamide **4d** (80 mg, 0.21 mmol, 1.0 equiv) in CH_2Cl_2 (5 mL) and 4-methoxybenzyl mercaptan (161.9 mg, 1.05 mmol, 5 equiv) gave **1df'** (70 mg, 63%) as dark brown oil. **^{1}H NMR** (400 MHz, $CDCl_3$): δ 7.77 (d, J = 8.5 Hz, 2H), 7.50 (d, J = 8.4 Hz, 2H), 7.17 (d, J = 8.5 Hz, 2H), 6.81 (d, J = 8.5 Hz, 2H), 6.35 (s, 1H), 4.22 (s, 2H), 3.77 (s, 3H), 3.60 (s, 2H), 3.55 (s, 2H). **^{13}C NMR** (101 MHz, CD_3OD): δ 160.2, 141.7 (determined by HMBC), 141.4, 140.4 (determined by HMBC), 139.5, 131.1, 129.6, 114.9, 100.5, 55.7, 38.3, 36.2, 25.1. **HRMS (ESI)**: Calcd. for $C_{18}H_{18}O_3N_4IS_2$ $[M-H]^-$ 528.9876; found 528.9835. **HPLC purity**: 96%

*4.1.3.9. 4-Iodo-N-((5-(methoxymethyl)-1H-1,2,3-triazol-4-yl)methyl)benzenesulfonamide (**1dg'**)*[14]. *N*-(4-azidobut-2-ynyl)-4-iodobenzenesulfonamide **4d** (106 mg, 0.28 mmol, 1.0 equiv) in methanol (2 mL) gave **1dg'** (101 mg, 88%) as colorless oil. **^{1}H NMR** (400 MHz, CD_3OD) δ 7.90 (d, J = 8.5 Hz, 2H), 7.54 (d, J = 8.5 Hz, 2H), 4.48 (s, 2H), 4.22 (s, 2H), 3.33 (s, 3H). **^{13}C NMR** (101 MHz, CD_3OD) δ 143.1 (determined from HMBC), 142.7 (determined from HMBC), 141.5, 139.5, 129.6, 100.4, 65.5, 58.7, 38.1. **HRMS (ESI)**: Calcd. for $C_{11}H_{13}O_3N_4IS$ $[M + H]^+$ 409.9861; found 409.9848. **HPLC purity**: 98%

*4.1.3.10. 4-Iodo-N-((5-(isopropoxymethyl)-1H-1,2,3-triazol-4-yl)methyl) benzenesulfonamide (**1dh'**)*[13]. *N*-(4-azidobut-2-ynyl)-4-iodobenzenesulfonamide **4d** (80 mg, 0.212 mmol, 1.0 equiv), in isopropanol (2 mL) gave **1dh'** (99 mg, 86%) as colorless oil. **^{1}H NMR** (400 MHz, CD_3OD): δ 7.95 – 7.89 (m, 3H), 7.55 (d, J = 8.1 Hz, 2H), 4.55 (s, 2H), 4.23 (s, 2H), 3.76 – 3.61 (m, 1H), 1.18 (d, J = 6.1 Hz, 6H). **^{13}C NMR** (101 MHz, CD_3OD): δ 141.4, 140.8 (2 × triazole C, determined from HMBC), 139.5, 129.6, 100.5, 73.2, 60.9, 49.0, 38.0, 22.2. **HRMS (ESI)**: Calcd. for $C_{13}H_{17}O_3N_4SINa$ $[M + Na]^+$ 458.9958; found 458.9958. **HPLC purity**: 95%

*4.1.3.11. N-((5-((benzylamino)methyl)-1H-1,2,3-triazol-4-yl)methyl)-4-iodobenzenesulfonamide (**1di'**)*. *N*-(4-azidobut-2-ynyl)-4-iodobenzenesulfonamide **4d** (100 mg, 0.26 mmol, 1.0 equiv), phenylmethanamine (139.0 mg, 1.3 mmol, 3 equiv) in CH_2Cl_2 (5 mL) gave **1di'** (95 mg, 72%) as colorless oil. **^{1}H NMR** (400 MHz, $CDCl_3$): δ 7.74 (d, J = 8.4 Hz, 2H), 7.46 (d, J = 8.4 Hz, 2H), 7.39 – 7.26 (m, 5H), 4.15 (s, 2H), 3.86 (d, J = 8.2 Hz, 4H). **^{13}C NMR** (101 MHz, $CDCl_3$): δ 140.9 (triazole, determined by HMBC), 140.6 (triazole, determined by HMBC), 139.7, 138.4, 137.1, 128.9, 128.6, 128.1, 100.0, 53.1, 42.5, 38.1. **HRMS (ESI)**: Calcd. for $C_{20}H_{23}O_2N_2IS$ $[M-H]^-$ 482.0146; found 482.0519.

*4.1.3.12. (4-((4-iodophenylsulfonamido)methyl)-1H-1,2,3-triazol-5-yl) methyl acetate (**1dj'**)*. N-(4-azidobut-2-ynyl)-4-iodobenzenesulfonamide **4d** (300 mg, 0.80 mmol, 1.0 equiv) and H_2O (2 mL) were heated at 60 °C overnight. The reaction mixture was evaporated to yield crude 5-hydroxymethyl triazole. A small portion of the crude was taken and acylated as follows. 5-Hydroxymethyl triazole (50 mg, 0.13 mmol, 1.0 equiv), Et_3N (55 µl, 0.39 mmol, 3.0 equiv), DMAP (1.5 mg, 0.013 mmol, 10 mol%) and acetic anhydride (12 µl, 0.13 mmol,1.0 equiv) were stirred in CH_2Cl_2 (20 mL/mmol of triazole) for 15–30 min (reaction was monitored by TLC). The reaction mixture was evaporated and purified by column chromatography to yield **1dj'** (31 mg, 54%) as colorless solid. **^{1}H NMR** (400 MHz, CD_3OD): δ 7.98 – 7.84 (m, 2H), 7.62 – 7.49 (m, 2H), 5.12 (s, 2H), 4.24 (s, 2H), 2.04 (s, 3H). **^{13}C NMR** (101 MHz, CD_3OD): δ 172.3, 141.5 (2*C; triazole, determined by HMBC), 140.8 (triazole, determined by HMBC), 139.5, 129.5, 100.5, 57.1, 37.9, 20.6. **HRMS (ESI)**: Calcd. for $C_{12}H_{14}O_4N_4SI$ $[M + H]^+$ 436.9775; found 436.9775. **HPLC purity**: 89%

4.2. Biological activity

4.2.1. Gene constructs of VIM-2, NDM-1 and GIM-1

In this study two types of gene constructs were used. The first included the native leader sequence to allow the proteins to be transported to the periplasm, for the three enzymes VIM-2 from *Pseudomonas aeruginosa* strain 301–5473 (GenBank no Q9K2N0), GIM-1 from *P. aeruginosa* (GenBank no Q704V1; [19,34]) and NDM-1 (GenBank no. E9NWK5, e.g [35,36]), where the latter bla_{NDM-1} gene is reported from several organisms. Cloning of bla_{NDM-1} or bla_{GIM-1} genes into the *Escherichia coli* pET26b(+) vector (Novagen) was performed using the primers and restriction cutting as described for VIM-26.[37] Cloning of bla_{VIM-2} into pET26b(+) is described previously.[38] The obtained *E. coli* pET-26b(+) MBL constructs were further used in the in the whole cell-based inhibitor assays.

In the second set of gene constructs used for the recombinant gene expression, the native leader sequence was removed and replaced with a *hexa*-His tag and a TEV cleavage site as reported earlier for VIM-2 (residues V27-E268;[17]) and GIM-1 (residues Q19-D250;[19]) both in pDEST14. NDM-1 used a codon optimized synthetic gene (Life Technologies, Thermo Fisher Scientific), with a TEV cleavage site with sequence ENLYFQG and residues G36-R280 in NDM-1 transformed in pDONR™221, and further sub cloned into pDEST17 with carries an *N*-terminal hexa His-tag, yielding pDest17-NDM-1 construct. Herein the residue numbering is the class B β-lactamase numbering scheme will be applied.[39]

4.2.2. Recombinant protein expression and purification of VIM-2, GIM-1 and NDM-1

The proteins were expressed and purified following this protocol. pDest17-NDM-1 was transformed into *E. coli* BL21 Star (DE3) pLysS (Invitrogen), and pDEST14 plasmids with VIM-2 or GIM-1 were transformed into in-house modified *E. coli* BL21 Star (DE3) pLysS (Invitrogen) cells with the pRARE plasmid (Novagen) in order to allow expression of genes encoding tRNAs for rare codons.[40] Precultures grown in Terrific Broth (TB) media with 100 μg/ml ampicillin (Sigma-Aldrich) and 34 μg/ml chloramphenicol (Sigma-Aldrich). The precultures were inoculated to 2 L Luria-Bertani (LB) media containing 100 μg/ml ampicillin and 34 μg/ml chloramphenicol and grown at 37 °C to reach an optical density (OD_{600} nm) of 0.5–1.0 before induced expression with 0.4 mM isopropyl β-D-1-thigalactopyranoside (IPTG; Sigma-Aldrich). The induced cultures were grown overnight at 20 °C before collecting the cells by centrifugation (8,900 X g, 30 min, 4 °C). Buffer A containing 50 mM HEPES pH 7.2, 100 μM $ZnCl_2$ and 150 mM NaCl was used to resuspend the cell pellets, following sonication and collecting the supernatants by centrifugation (3000 g, 40 min, 4 °C). The recombinant proteins were affinity purified using a 1 mL or 5 mL His-Trap HP column (GE Healthcare) in buffer A washed with 5% buffer B (50 mM HEPES pH 7.2, 100 μM $ZnCl_2$, 150 mM NaCl and 1 M imidazole), before eluted in a gradient of 5 to 100% buffer B. Peak fractions were investigated using 4–20% sodium dodecyl sulfate polyacrylamide gel electrophoresis (SDS-PAGE; Bio-Rad).[41] The fractions containing MBL protein was added in-house-made His-tagged TEV protease in a 1:100 mg ratio of TEV:protein and dialyzed at 4 °C overnight using 10-kDa cutoff Snakeskin (Pierce) in buffer C (50 mM HEPES pH 7.2, 150 mM NaCl, 1 mM EDTA and 1 mM β-mercaptoethanol). To remove uncleaved protein and TEV protease a second His-Trap purification was performed. SDS-PAGE analysis was used to estimate a purity of ~ 95% of the fractions containing protein, which then were pooled and dialyzed in buffer A overnight.

4.2.3. Dose rate inhibition studies for IC_{50} determination

The half-maximal inhibitory concentration (IC_{50}) against the VIM-2, NDM-1 and GIM-1 enzymes were determined by using sixteen different concentration of inhibitor compounds ranging from 0 μM to 250 μM. A 100 μl solution with 50 mM HEPES buffer (pH 7.2), 100 μM $ZnCl_2$), purified enzyme (1 nM VIM-2, NDM-1 or GIM-1) and 2.5–0 mM inhibitor was incubated in a 96 well plate at 25 °C for 5 min. In addition, the enzyme buffer contained 400 μg/ml Bovine Serum Albumin (BSA) to prevent protein unfolding and loss of activity due to low concentrations.[42,43] 100 μM of the reporter substrate nitrocefin (VIM-2, GIM-1) or imipenem (NDM-1) was added to the enzyme-inhibitor solution and the increase in absorbance at 482 nm (nitrocefin) or 300 nm (imipenem) was recorded on a Spectramax M2e spectrophotometer (Molecular Devices). Each data point was performed in triplicates and the initial velocity for each inhibitor concentration was analysed by a log [inhibitor] vs. response curve fitting to calculate IC_{50} in GraphPad Prism 5.0 software.

4.2.4. Cell-based screening assay of the inhibition potential

The inhibitory activity of the inhibitors was investigated in a cell-based assay using a β-lactamase-negative *E. coli* SNO3 (ampA1 ampC8 pyrB recA rpsL)[44] transformed with pET26b(+) containing bla_{VIM-2}, bla_{GIM-1} or bla_{NDM-1}. The screen was conducted in 96-well plates (Corning) in duplicates. 50 μl overnight culture (adjusted to an OD_{600} of 1 in LB broth) of E. coli SNO3 containing one of the MBLs, inhibitor (with a final concentration of 250 μM), 0.8 mM (final concentration) Isopropyl ß-D-1-thiogalactopyranoside (Sigma, IPTG) and 50 μl LB media, were added to each well. The plate was incubated at 37 °C for 20 min with shaking to induce the expression of the MBL. Subsequently, 50 μl nitrocefin (diluted in 50 mM HEPES pH 7.2 and 100 μM $ZnCl_2$ to give a final concentration of 1.6 mM in the assay) was added. Nitrocefin hydrolysis was measured at OD_{482} every minute for 3 h with shaking (47 s) in between reads using a Spectramax M2^e spectrophotometer (Molecular Devices). EDTA (250 μM concentration) was used as positive control and wells containing no inhibitor as negative controls. The percent inhibition was calculated according to equation 1.

$$\% \text{ inhibition} = \frac{\text{Slope (No inhibitor)} - \text{Slope (Inhibitor)}}{\text{Slope (No inhibitor)}} \times 100\% \quad \text{equation} \quad (1)$$

The synergistic effect of the inhibitors with meropenem was tested against selected clinical bacterial strains containing MBLs. The bacterial strains were plated on lactose agar plates with 100 mg/L ampicillin and lactose agar and incubated overnight at 37 °C. The inhibitors were diluted to a final concentration of 50 μM (**1cc'**, **1dh'**, **1dh'**, **1di'**,**1dj'**) or 125 μM (**1dd'**, **1dc'**) in Mueller Hinton (MH) broth. In order to monitor the effect of the DMSO in the assay, a DMSO control was included with a concentration of 5%. Meropenem was diluted in MH broth in a 2-fold dilution series with final concentrations of 256 μg/mL − 0.0625 μg/mL. The microtiter plates were inoculated with a 0.5 McFarland suspension of the bacterial strain in 0.85% NaCl, which were diluted in MH broth. A quality check of bacterial suspension in 0.85% NaCl in a 1:100 ratio was incubated on MH agar plates overnight at 37 °C. The final CFU/mL inoculum were calculated and compared to a standard. The microtiter plates were incubated for 20 h at 37 °C. The minimum inhibitory concentrations (MIC) were detected by visual inspection of the plates the next day.

4.3. Crystallization, X-ray data collection and data analysis

The DMSO-free co-crystallization method[45] was used to crystallize VIM-2 in complex with the inhibitor **1cc'**, **1dh'** and **1di'**. In brief, the inhibitors were dissolved in DMSO and used to pre-coat the reservoir wells of an MRC-96-well crystallization plate (Molecular Dimensions) by DMSO evaporating. Reservoir solution consisting of 22–27% polyethylene glycol (PEG) 3350 and 0.2 M magnesium formate was added to every well and incubated for 24 h. The reservoir solution was mixed with the protein solution (9.4 mg/ml) in a 1:1 ratio and used for sitting-drop experiments. Protein crystals were harvested after 1–2 weeks.

Soaking of native VIM-2 crystals was used for the crystallization of

VIM-2 in complex with the inhibitor **1dj'**.[17] The native VIM-2 crystals were grown using the hanging drop-method and reservoir solution consisting of 22–27% PEG 3350 and 0.2 M magnesium formate. **1dj'** was dissolved in DMSO at a concentration of 100 mM. The native VIM-2 crystals were transferred to reservoir solution containing 2.5 mM **1dj'**and harvested after 12 h.

After harvesting, all crystals were transferred to 25% PEG 3350, 0.2 M $MgCl_2$, 15% ethylene glycol, 50 mM HEPES pH 7.2 and flash cooled in liquid nitrogen. The collection of the X-ray data was carried out at the ID23-1 or ID-29 at the European Synchrotron Radioation Facility (ESRF) in Grenoble, France. The data sets were integrated, scaled and truncated using XDS,[46] POINTLESS and AIMLESS.[47,48] Molecular replacement was carried out using PHASER[49] with a previously published VIM-2 structure (PDB: 1KO3).[28] Several refinement cycles in PHENIX[50] and molecular modeling in WinCoot[51] according to the 2Fo-Fc and Fo-Fc map were used to obtain the final structure. For the complex structures with the inhibitors **1dh'** and **1cc'**, all atoms except water were refined with anisotropic B-factors. For the complex structures with **1di′** and **1dj′**, TLS parameters and anisotropic B-factors refinement for Zn^{2+} and Cl^- were applied. R-free cross validation was done with 5% of the data. Conditions for the data collection and refinement statistics are shown in Table 1. The PyMOL Molecular Graphic System, version 1.4.1. (Schrödinger), and LIGPLOT[33] were used to generate illustrations and visualize interactions.

4.3.1. PDB accession codes

Coordinates and structure factors of have all been deposited in the Protein Data Bank with accession numbers 6TMC (VIM-2_**1dh'**), 6TM9 (VIM-2_**1cc'**), 6TMB (VIM-2_**1di'**) and 6TMA (VIM-2_**1dj'**).

Declaration of Competing Interest

The authors declare that they have no known competing financial interests or personal relationships that could have appeared to influence the work reported in this paper.

Acknowledgements

This work was supported by the Tromsø Research Foundation and the Research Council of Norway (project numbers 218539, SYNKNOYT 2011, 213808, FRIMEDBIO 2011 and 273332/2018), and this is highly acknowledged. The provision of beam time at ID23-1 and ID29, ESRF, Grenoble are highly valued. We acknowledge Trine Josefine O. Carlsen for purification and help with crystallization of proteins. Silje Lauksund and Ørjan Samuelsen are both acknowledged for synergy testing.

Appendix A. Supplementary data

Supplementary data to this article can be found online at https://doi.org/10.1016/j.bmc.2020.115598.

References

1. WHO, 2014, ISBN-978-992-974-156474-156478.
2. Patel G, Bonomo RA. *Front Microbiol.* 2013;4:48.
3. Walsh TR. *Int J Antimicrob Agents.* 2010;36:S8–S14.
4. Docquier J-D, Mangani S. *Drug Resist Updat.* 2018;36:13–29.
5. Bush K, Bradford PA. *Nat Rev Microbiol.* 2019;17:295–306.
6. Toussaint KA, Gallagher JC. *Ann Pharmacother.* 2015;49:86–98.
7. Everett M, Sprynski N, Coelho A, et al. *Antimicrob Agents Chemother.* 2018;62:e00074–00018.
8. King AM, Reid-Yu SA, Wang W, et al. *Nature.* 2014;510:503–506.
9. Yang SK, Kang JS, Oelschlaeger P, Yang KW, Med ACS. *Chem Lett.* 2015;6:455–460.
10. González MM, Kosmopoulou M, Mojica MF, et al. *ACS Infect Dis.* 2015;1:544–554.
11. Spyrakis F, Celenza G, Marcoccia F, et al. *Chem Lett.* 2018;9:45–50.
12. Sevaille L, Gavara L, Bebrone C, et al. *ChemMedChem.* 2017;12:972–985.
13. Weide T, Saldanha SA, Minond D, et al. *Chem Lett.* 2010;1:150–154.
14. Minond D, Saldanha SA, Subramaniam P, et al. *Bioorg Med Chem.* 2009;17:5027–5037.
15. Skagseth S, Akhter S, Paulsen MH, et al. *Eur J Med Chem.* 2017;135:159–173.
16. Christopeit T, Yang K-W, Yang S-K, Leiros H-KS. *Acta Crystallogr F Struct Biol Commun.* 2016;72:813–819.
17. Christopeit T, Carlsen TJ, Helland R, Leiros H-KS. *J Med Chem.* 2015;58:8671–8682.
18. Zhang H, Hao Q. *FASEB J.* 2011;25:2574–2582.
19. Borra PS, Samuelsen Ø, Spencer J, Walsh TR, Lorentzen MS, Leiros H-KS. *Antimicrob Agents Chemother.* 2013;57:848–854.
20. Loren JC, Sharpless KB. *Synthesis.* 2005;9:1514–1520.
21. Banert K. *Chem Ber.* 1989;122:911–918.
22. Banert K, Hagedorn M, Hemeltjen C, Ihle A, Weigand K, Priebe H. *Arkivoc.* 2016;2016:338–361.
23. Banert K, Hagedorn M. *Angew Chem Int Ed Engl.* 1989;28:1675–1676.
24. Alexander JR, Packard MH, Hildebrandt AM, Ott AA, Topczewski JJ. *J Organic Chem.* 2020;85:3174–3181.
25. Christopeit T, Leiros H-KS. *Bioorg Med Chem Lett.* 2016;26:1973–1977.
26. Yamaguchi Y, Jin W, Matsunaga K, et al. *J Med Chem.* 2007;50:6647–6653.
27. Aitha M, Marts AR, Bergstrom A, et al. *Biochemistry.* 2014;53:7321–7331.
28. Garcia-Saez I, Docquier JD, Rossolini GM, Dideberg O. *J Mol Biol.* 2008;375:604–611.
29. Leiros H-KS, Timmins J, Ravelli RB, McSweeney SM. *Acta Crystallogr D Biol Crystallogr.* 2006;62:125–132.
30. Ravelli RB, Leiros H-KS, Pan B, Caffrey M, McSweeney S. *Structure.* 2003;11:217–224.
31. Leiros HK, McSweeney SM, Smalas AO. *Acta Crystallogr D Biol Crystallogr.* 2001;57:488–497.
32. Chen J, Liu YF, Cheng TY, et al. *Med Chem Res.* 2014;23:300–309.
33. Wallace AC, Laskowski RA, Thornton JM. *Protein Eng.* 1995;8:127–134.
34. Castanheira M, Toleman MA, Jones RN, Schmidt FJ, Walsh TR. *Antimicrob Agents Chemother.* 2004;48:4654–4661.
35. Yong D, Toleman MA, Giske CG, et al. *Antimicrob Agents Chemother.* 2009;53:5046–5054.
36. Kumarasamy KK, Toleman MA, Walsh TR, et al. *Lancet Infect Dis.* 2010;10:597–602.
37. Leiros H-KS, Edvardsen KS, Bjerga GE, Samuelsen Ø. *FEBS J.* 2015;282:1031–1042.
38. Samuelsen Ø, Castanheira M, Walsh TR, Spencer J. *Antimicrob Agents Chemother.* 2008;52:2905–2908.
39. Garau G, Bebrone C, Anne C, Galleni M, Frere JM, Dideberg O. *J Mol Biol.* 2005;345:785–795.
40. E. A. Rogulin, T. A. Perevyazova, L. A. Zheleznaya and N. I. Matvienko, Biochemistry-Moscow +, 2004, 69, 1123-1127.
41. Laemmli UK. *Nature.* 1970;227:680–685.
42. Laraki N, Franceschini N, Rossolini GM, et al. *Antimicrob Agents Chemother.* 1999;43:902–906.
43. Siemann S, Evanoff DP, Marrone L, Clarke AJ, Viswanatha T, Dmitrienko GI. *Antimicrob Agents Chemother.* 2002;46:2450–2457.
44. Sun Q, Law A, Crowder MW, Geysen HM. *Bioorg Med Chem Lett.* 2006;16:5169–5175.
45. Christopeit T, Albert A, Leiros H-KS. *Bioorg Med Chem.* 2016;24:2947–2953.
46. Kabsch W. *Acta Crystallogr D Biol Crystallogr.* 2010;66:125–132.
47. Evans PR. *Acta Crystallogr D Biol Crystallogr.* 2011;67:282–292.
48. Evans P. *Acta Crystallogr D Biol Crystallogr.* 2006;62:72–82.
49. McCoy AJ, Grosse-Kunstleve RW, Adams PD, Winn MD, Storoni LC, Read RJ. *J Appl Crystallogr.* 2007;40:658–674.
50. Adams PD, Afonine PV, Bunkoczi G, et al. *Acta Crystallogr D Biol Crystallogr.* 2010;D66:213–221.
51. Emsley P, Lohkamp B, Scott WG, Cowtan K. *Acta Crystallogr D Biol Crystallogr.* 2010;66:486–501.